NOTCH signaling in skeletal progenitors is critical for fracture repair

Cuicui Wang,[1,2] Jason A. Inzana,[1,3] Anthony J. Mirando,[1,4] Yinshi Ren,[4] Zhaoyang Liu,[1,5] Jie Shen,[1,6] Regis J. O'Keefe,[1,6] Hani A. Awad,[1,3] and Matthew J. Hilton[1,4,7]

[1]Department of Orthopaedics and Rehabilitation, The Center for Musculoskeletal Research, University of Rochester Medical Center, and [2]Department of Pathology and Laboratory Medicine, University of Rochester Medical Center, Rochester, New York, USA. [3]Department of Biomedical Engineering, University of Rochester, Rochester, New York, USA. [4]Department of Orthopaedic Surgery, Duke Orthopaedic Cellular, Developmental, and Genome Laboratories, Duke University School of Medicine, Durham, North Carolina, USA. [5]Department of Biology, University of Rochester, Rochester, New York, USA. [6]Department of Orthopedic Surgery, Washington University School of Medicine, St. Louis, Missouri, USA. [7]Department of Cell Biology, Duke Orthopaedic Cellular, Developmental, and Genome Laboratories, Duke University School of Medicine, Durham, North Carolina, USA.

Fracture nonunions develop in 10%–20% of patients with fractures, resulting in prolonged disability. Current data suggest that bone union during fracture repair is achieved via proliferation and differentiation of skeletal progenitors within periosteal and soft tissues surrounding bone, while bone marrow stromal/stem cells (BMSCs) and other skeletal progenitors may also contribute. The NOTCH signaling pathway is a critical maintenance factor for BMSCs during skeletal development, although the precise role for NOTCH and the requisite nature of BMSCs following fracture is unknown. Here, we evaluated whether NOTCH and/or BMSCs are required for fracture repair by performing nonstabilized and stabilized fractures on NOTCH-deficient mice with targeted deletion of *RBPjk* in skeletal progenitors, maturing osteoblasts, and committed chondrocytes. We determined that removal of NOTCH signaling in BMSCs and subsequent depletion of this population result in fracture nonunion, as the fracture repair process was normal in animals harboring either osteoblast- or chondrocyte-specific deletion of *RBPjk*. Together, this work provides a genetic model of a fracture nonunion and demonstrates the requirement for NOTCH and BMSCs in fracture repair, irrespective of fracture stability and vascularity.

Introduction

Although most fractures progress to union, 10% to 20% result in nonunions and are often associated with morbidity, prolonged hospitalization, and increased expenses (1–3). Risk factors for fracture nonunion can include malnutrition, infection, metabolic disease, poor vascularization or vascular disease, fracture comminution, and most commonly, inappropriate fixation or stabilization at the fracture site (4). However, there remain questions as to whether systemic factors or impaired cellular function may play a role in the pathogenesis of fracture nonunion, particularly in cases that do not heal after appropriate surgical intervention. A reduced pool of human bone marrow stromal/stem cells (BMSCs) correlates with altered bone repair in patients with fracture nonunions (5, 6). The administration of BMSCs has shown promise in treating patients with fracture nonunions in some settings (7–12). Interestingly, recent studies using reporter-tagged BMSCs have demonstrated that transplanted BMSCs specifically localize within the fracture gap and intramedullary or internal calluses rather than within the external callus tissues mostly derived from the periosteum and surrounding soft tissue, suggesting a localized and specific role for BMSCs in fracture repair (13, 14). While the importance of BMSC-associated osteogenesis during development has been established, the functional role and importance of BMSCs in fracture healing remain to be determined.

Through the use of mouse genetic studies, we and others have demonstrated that loss of NOTCH signaling in skeletal progenitors leads to an early increase in bone mass, depletion of the BMSC pool, and subsequent age-related bone loss (15, 16). The NOTCH signaling pathway is a known regulator of various stem cell populations that signals via single-pass transmembrane ligands (JAG1/2 and DLL1/3/4) and receptors (NOTCH1/4), culminating in the activation of a transcriptional complex composed of the NOTCH intracellular domain (NICD), the mastermind-like transcriptional coactivator (MAML), and the central regulator known as recombination binding protein for immunoglobulin kappa J region (RBPjκ) (17). Although NOTCH signaling is critical for maintaining BMSCs during skeletal development (15, 16), little evidence exists for a particular role for NOTCH signaling during fracture repair. Here, we set out to test the hypothesis that NOTCH signaling in skeletal progenitors serves to preserve the numbers and maintain the progenitor status of BMSC populations that are critical for normal fracture repair and unification, while NOTCH signaling within more committed skeletal lineages may be largely dispensable.

Note regarding evaluation of this manuscript: Manuscripts authored by scientists associated with Duke University, The University of North Carolina at Chapel Hill, Duke-NUS, and the Sanford-Burnham Medical Research Institute are handled not by members of the editorial board but rather by the science editors, who consult with selected external editors and reviewers.

Conflict of interest: The authors have declared that no conflict of interest exists.

Submitted: December 22, 2014; **Accepted:** January 21, 2016.

Reference information: *J Clin Invest*. 2016;126(4):1471–1481. doi:10.1172/JCI80672.

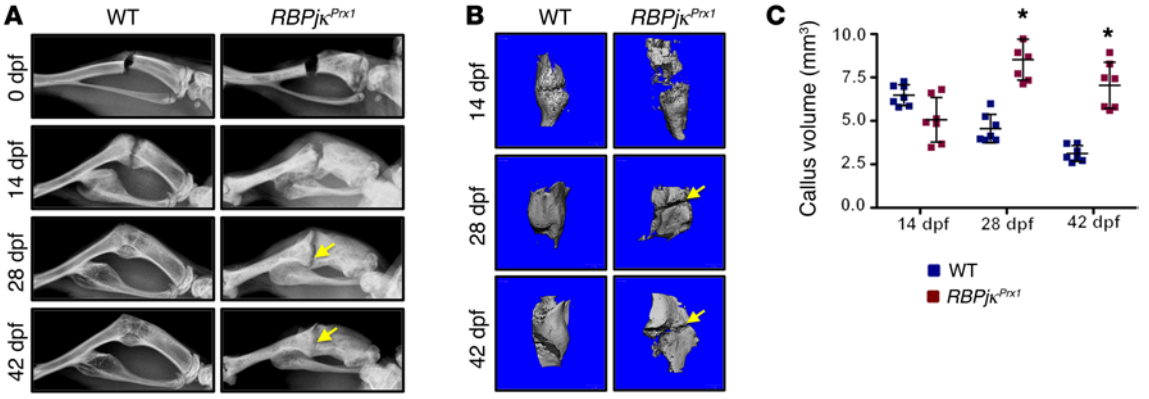

Figure 1. Loss of NOTCH signaling in MSCs results in fracture nonunion. (**A**) A real-time radiographic comparison of 2 representative nonstabilized tibia fractures from WT and *RBPjκ*^{Prx1} mutant mice at 0, 14, 28, and 42 dpf revealed persistent fracture lines (yellow arrows) at 42 dpf, suggesting an established fracture nonunion in *RBPjκ*^{Prx1} mutants. *n* = 12 mice per genotype per time point. (**B**) μCT analyses of 14-, 28-, and 42-day-old WT and *RBPjκ*^{Prx1} mutant fractures revealed substantial periosteal external callus formation by 14 dpf and beyond, but apparent radiolucent space (yellow arrows) between broken cortices at 42 dpf in *RBPjκ*^{Prx1} mutants. *n* = 7 mice per genotype per time point. (**C**) Reconstruction of μCT data reflected the normal and robust periosteal response in *RBPjκ*^{Prx1} mutants; however, the new bone remodeling was delayed in these animals. *n* = 7 mice per genotype per time point. **P* < 0.05 compared with WT by 2-way ANOVA followed by Dunnett's post hoc test. Results are expressed as mean ± SD.

Results

Loss of NOTCH signaling in skeletal progenitors results in fracture nonunion. To examine the role of NOTCH signaling during fracture repair, we generated a loss-of-function (LOF) mouse model in which floxed alleles for the transcriptional NOTCH effector RBPjκ were conditionally deleted in skeletal progenitors. Western blot analyses confirmed that RBPjκ was efficiently deleted in the skeletal lineages of *Prx1-Cre RBPjk*$^{fl/fl}$ (herein referred to as *RBPjκ*^{Prx1}) mice at 2 months of age (Supplemental Figure 1; supplemental material available online with this article; doi:10.1172/JCI80672DS1). To identify the cell lineages targeted by *Prx1-Cre* and contribute to callus formation during fracture repair, we analyzed tibia fractures on *Prx1-Cre R26RLacZ* mice at 14 days post fracture (dpf). X-gal staining on fracture calluses revealed LacZ-positive cells in the periosteum, the BM of the diaphysis, and both the external and internal cartilaginous and bony callus (Supplemental Figure 2). These data demonstrate that all skeletal-related cells in the callus are derived from *Prx1*-expressing progenitors, which largely reside in both the periosteum and BM.

To determine whether normal fracture repair requires a NOTCH-maintained population of BMSCs, we performed nonstabilized tibia fractures on *RBPjκ*^{Prx1} (largely depleted of the clonogenic fraction of BMSCs) and WT control mice at 2 months of age. Radiographs of WT fractures demonstrated the initial signs of external callus forming by 14 dpf, followed by the disappearance of the cortical gap via a bridging internal and external bony callus by 28 dpf, indicating fracture unification. In contrast, *RBPjκ*^{Prx1} mutant fractures showed prominent callus formation along the periosteum extending away from the fracture line at 14 and 28 dpf; however, no bridging callus between the cortices was observed. Radiographic observations out to 42 dpf demonstrated a clear nonunion of *RBPjκ*^{Prx1} mutant tibiae (Figure 1A). Consistent with radiographic data, μCT analyses on mineralized calluses of WT fractures showed a nearly complete bridging of bony calluses by 14 dpf, followed by complete bridging at 28 dpf and beyond. *RBPjκ*^{Prx1} fractures presented with a large radiolucent space between broken cortices at 14 dpf that remained evident up to and beyond 42 dpf (Figure 1B). Reconstruction of μCT data revealed that mineralized callus volumes in WT fractures peaked at 14 dpf and rapidly decreased from 14 dpf to 42 dpf, suggesting continuous external callus remodeling. Quantitatively, substantial new external callus bone formation was observed in *RBPjκ*^{Prx1} mutant fractures, reflecting relatively normal and robust periosteal and soft tissue responses in these mutants. In contrast, bone remodeling was likely delayed in *RBPjκ*^{Prx1} mutant fractures, since callus volumes did not show a decline until beyond 28 dpf (Figure 1C).

A fibrous hypertrophic nonunion develops in RBPjκ^{Prx1} *mutant fractures*. Histological assessments of fracture repair were performed using alcian blue/hematoxylin/orange-g (ABH/OG) staining of *RBPjκ*^{Prx1} mutant and WT fracture calluses at 7, 14, 28, and 42 dpf (Figure 2A). At 7 dpf, WT and *RBPjκ*^{Prx1} mutant fracture calluses were comparable, with early signs of mesenchymal cell recruitment, cartilage formation in the external calluses, and the appearance of vascular tissue noted by the presence of red blood cells (Figure 2A). By 14 dpf, further callus formation in WT fractures was observed in 3 areas, including (a) the endosteal surface close to the fracture rim and within the intramedullary BM space, (b) the fracture gap directly adjacent to the fractured cortices, and (c) the periosteal surface of both proximal and distal sides of the tibiae, where the transition from cartilaginous to bony callus was nearly complete. By 28 dpf, the cortices in WT fractures were unified by bridging calluses in both the periosteal and intramedullary areas. Due to bony union and new bone remodeling, WT fractures were completely repaired, as illustrated by the restoration of the original lamellar structure of the cortical bone by 42 dpf (Figure 2A). Alternatively at 14 dpf, *RBPjκ*^{Prx1} mutants exhibited no internal callus formation, but rather displayed a persistence of undifferentiated mesenchymal tissue within both the intramedullary space and the fracture gap. Interestingly, relatively normal external callus formation could be visualized along the periosteal surfaces, although the replacement of cartilage by bone was delayed, suggesting the periosteal-derived stem/progenitor cell (PSC) popu-

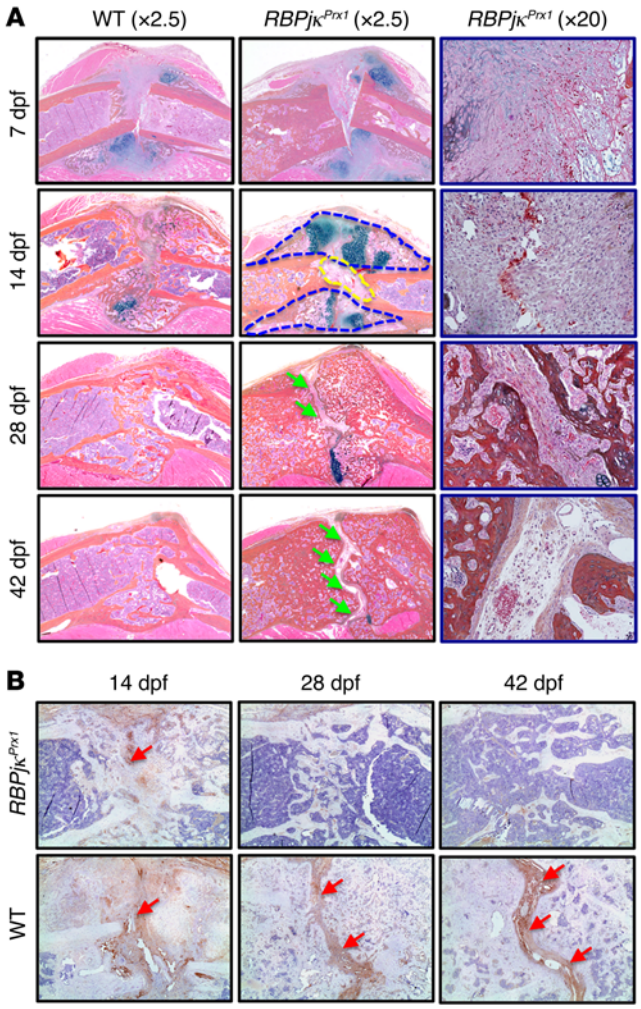

Figure 2. Loss of NOTCH signaling in MSCs results in histological changes consistent with the pathology of fracture nonunion. (**A**) ABH/OG-stained callus sections from WT and *RBPjκ*^{Prx1} mutants at 7, 14, 28, and 42 dpf showed prominent external callus formation (blue dotted line area) and persistent mesenchymal tissue (yellow dotted line area) within the internal callus area, which was ultimately filled with mesenchymal fibrous tissue (green arrows) in *RBPjκ*^{Prx1} mutant fractures. Mesenchymal/fibrotic callus regions are shown at high magnification in blue boxes. n = 5 mice per genotype per time point. (**B**) IHC for COL3A1 on callus sections from WT and *RBPjκ*^{Prx1} mutant fractures at 14, 28, and 42 dpf confirmed the formation of mesenchymal-like fibrous tissue in the fracture gap of *RBPjκ*^{Prx1} mutants. n = 5 mice per genotype per time point. Original magnification, ×5. Red arrows indicate the expression of COL3A1.

lation was largely unaffected in *RBPjκ*^{Prx1} mutant mice. By 28 dpf and beyond, regions of the intramedullary space and fracture gap mostly were filled with mesenchymal fibrous tissue (Figure 2A). To determine the fibrotic nature of the mesenchymal tissue that developed and persisted at the fracture site, we performed immunohistochemistry (IHC) for COL3A1 (Figure 2B). COL3A1 expression, which was minimally visualized in WT fracture sections at 14 dpf, dissipated over time, as it does during normal fracture repair. Alternatively, COL3A1 appeared to be more pronounced over the course of healing in *RBPjκ*^{Prx1} mutant fracture sections, especially within the fracture gap and the intramedullary mesenchymal area, confirming that a fibrous nonunion developed in these mutant mice (Figure 2B).

We next performed quantitative assessments of tissue composition of fracture calluses to further understand fracture healing in these mice. Consistent with histological observations, histomorphometric results revealed that the cartilage and bone areas were significantly increased in *RBPjκ*^{Prx1} mutant fractures throughout much of the fracture repair process, which was attributed to the robust endochondral bone formation that occurred along the periosteal surfaces as well as the delayed bone remodeling (Figure 3A). The significantly greater amount of mesenchymal tissue observed throughout the healing process in *RBPjκ*^{Prx1} mutant fractures mostly appeared within the internal or intramedullary callus area and ultimately caused the lack of any bone unification (Figure 3A). To determine the structural impact of the altered fracture-healing processes, we analyzed fractured WT and *RBPjκ*^{Prx1} mutant tibiae at 42 dpf using biomechanical torsion testing. As expected, all biomechanical parameters, including bone strength, bone stiffness, and bone toughness, were markedly lower in *RBPjκ*^{Prx1} mutant tibiae (~7-fold lower, $P \leq 0.002$) (Figure 3B). No failure moment could be specifically detected in *RBPjκ*^{Prx1} mutant tibiae, indicating the complete absence of any rigid unifying structure (Figure 3B). In addition, the minimal torsional stiffness possessed by *RBPjκ*^{Prx1} mutant fractured tibiae suggested soft tissue bridging of bone fragments, resulting in a slow tearing rather than abrupt breaking during tests (Figure 3B). The fully restored mechanical competence in the WT group, compared with nearly undetectable parameters in the mutant group, demonstrated not just delayed fracture repair, but rather an actual and complete nonunion.

The fracture nonunions observed in RBPjκ^{Prx1} *mutants are likely due to the depleted and/or defective BMSC pool, rather than altered vascularization or osteoclast numbers.* To determine whether alterations in vascularization contribute to fracture nonunions in *RBPjκ*^{Prx1} mutants, we performed PECAM immunofluorescence (IF) on callus sections at 14 dpf. In regions of the external callus, we observed similar patterns of vascularization between WT and mutant fractures. The cartilaginous tissue was avascular, and new blood vessels invaded areas of new bone formation, indicating normal endochondral bone healing within external calluses from both groups (Supplemental Figure 3, B and E). Within areas of internal calluses of WT fractures, we also observed that bone fragments were bridged by avascular cartilaginous tissue flanked by vascular tissue (Supplemental Figure 3, A and C). Surprisingly, abundant PECAM expression was observed across the fracture gap containing mesenchymal-like fibrous tissue without evidence of bone formation in *RBPjκ*^{Prx1} mutants (Supplemental Figure 3, D and F). Thus, it was unlikely that the fracture nonunions observed in *RBPjκ*^{Prx1} mutants could be attributed to a disrupted vascular network, since the tissues within the fracture gap were highly vascularized. Vascularization at all stages of fracture repair was further evidenced by the presence of red blood cells and vascular tissues within the intramedullary and fibrous tissue domains observed within the ABH/OG-stained histology sections from the *RBPjκ*^{Prx1} mutant fractures (Figure 2A). Additionally, tartrate resistant acid phosphatase (TRAP) staining for osteoclasts was also assessed to determine whether dysregulated osteoclastogenesis could be

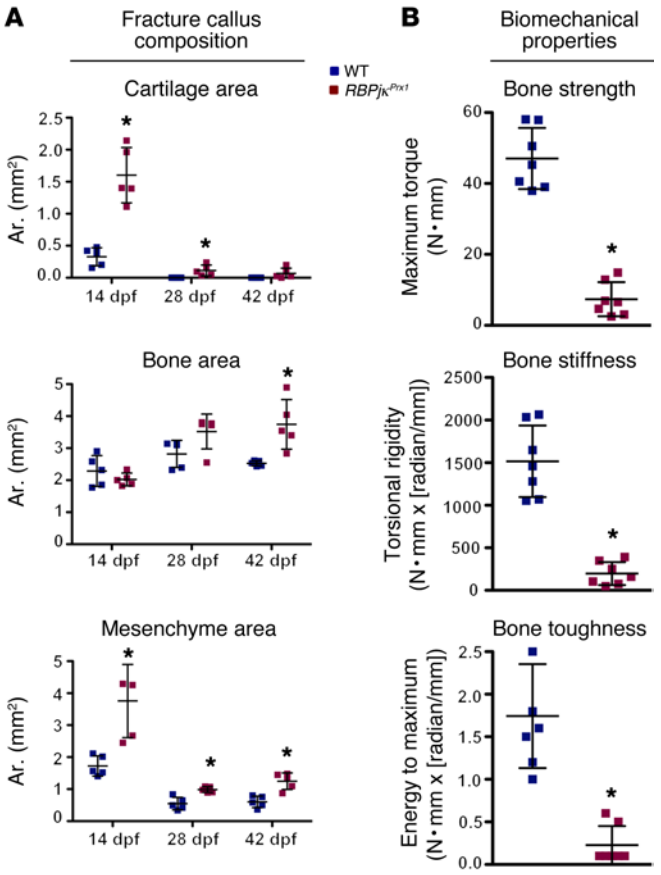

Figure 3. *RBPjκ*^{Prx1} mutant fractures have altered callus composition with remarkably inferior biomechanical properties. (**A**) Histomorphometric quantifications of the cartilage, bone, and mesenchymal areas (Ar.) from ABH/OG-stained sections show robust cartilage and bone formation in the external callus regions and the progression of fracture nonunion in *RBPjκ*^{Prx1} mutant fractures. n = 5 mice per genotype per time point. *P < 0.05 compared with WT by 2-way ANOVA followed by Dunnett's post hoc test. Results are expressed as mean ± SD. (**B**) Biomechanical torsion testing of WT and *RBPjκ*^{Prx1} mutant fractures at 42 dpf. All biomechanical parameters, including the maximum torque, torsional rigidity, and energy to maximum, which represent the bone strength, bone stiffness, and bone toughness, respectively, were markedly lower in *RBPjκ*^{Prx1} mutant repaired tibia than those in the WT controls. n = 7 mice per genotype. *P < 0.05 compared with WT by 2-tailed, unpaired Student's t test. Results are expressed as mean ± SD.

an underlying contributor to fracture nonunion. While the total number of TRAP-positive cells observed throughout mutant fracture sections was greater than that in WT controls (Supplemental Figure 4A), the percentage of bone surface covered by osteoclasts (OC.S./B.S.) was comparable or lower (Supplemental Figure 4B). Therefore, these data indicate that the fracture nonunions in *RBPjκ*^{Prx1} mutants are not caused by enhanced osteoclastogenesis.

Previous studies have demonstrated that loss of NOTCH signaling in skeletal progenitors significantly enhanced trabecular bone mass in adolescent mice at the expense of depleting the BMSC or skeletal progenitor pool (15, 16). We reasoned that the fracture nonunion observed in *RBPjκ*^{Prx1} mutants might be due to this significant reduction in BMSCs. Since skeletal progenitors are found in the clonogenic subset of adherent BM-associated cells identified by CFU assays, we isolated cells from WT and *RBPjκ*^{Prx1} mutant fractures at 42 dpf and assayed for CFU-fibroblastic (CFU-F) and CFU-osteoblastic (CFU-OB) frequency in BM-associated cells. Crystal violet staining of CFU-Fs and alkaline phosphatase (ALP) staining of CFU-OBs revealed remarkably fewer type I CFU-Fs and CFU-OBs in the BM of *RBPjκ*^{Prx1} mutant fractures (Figure 4, A and B), indicating a severe diminution of the clonogenic fraction of the BMSC pool. Interestingly, the ratio of CFU-OB to CFU-F was significantly higher in the BMSC cultures from *RBPjκ*^{Prx1} mutant fractures (Figure 4B), suggesting the remaining clonogenic BMSCs were less "stem-like" and more differentiated than those present in WT fractures. To determine the direct impact of NOTCH inhibition on clonogenic subsets of BMSCs, we performed CFU-F assays using BMSCs isolated from 2-month-old WT C57BL6/J mice treated with either 10 μM *N*-[(3,5-difluorophenyl)acetyl]-L-alanyl-2-phenyl]glycine-1,1-dimethylethyl ester (DAPT) (Calbiochem), a γ-secretase inhibitor that inhibits all NOTCH signaling, or DMSO as a control. Crystal violet staining of BMSC cultures with continuous NOTCH inhibition from days 3 to 17 after plating showed a dramatic reduction in type I CFU-Fs compared with that in DMSO-treated controls (Figure 4, C and D). Gene-expression analyses from these cultures demonstrated direct NOTCH inhibition in BMSCs via the downregulation of the NOTCH target gene hairy and enhancer of split 1 (*Hes1*) (Figure 4E). DAPT treatments subsequently resulted in a dramatic downregulation of leptin receptor (*Lepr*) expression (Figure 4E), which marks a critical subset of clonogenic BMSCs specifically derived from the intramedullary and endocortical BM and serves as an important skeletal progenitor source that contributes to normal fracture repair (18). Consistent with this reduction of skeletal progenitors or early osteogenic cells following 2 weeks of DAPT treatments, we observed a decrease in collagen type I alpha 1 (*Col1a1*) expression and a subsequent increase in *Alp* and osteocalcin (*Oc*) expression, suggesting that remaining cells were a more committed osteogenic cell population (Figure 4E). Collectively, these data argue that NOTCH signaling inhibition directly within skeletal progenitors results in a significant effect on BMSC populations, such that they lose their progenitor status with time and that, following fracture, *RBPjκ*^{Prx1} mutants likely form fibrous nonunions due to the depletion of BMSC populations with altered differentiation potential.

Loss of NOTCH signaling in osteoblasts or chondrocytes does not result in fracture nonunion. Thus far, we could not rule out the possibility that NOTCH-defective osteoblasts or chondrocytes contribute significantly to the nonunion phenotype observed in *RBPjκ*^{Prx1} mutant fractures, since the *Prx1-Cre* lineage traces to more committed osteoblast and chondrocyte populations during fracture repair (Supplemental Figure 2). Therefore, to determine whether loss of NOTCH signaling in osteoblasts could also lead to fracture nonunion, we first traced the fate of *Col1a1*(2.3 kb)–expressing osteoblastic cells during fracture repair by analyzing the fracture callus of *Col1a1-Cre*(2.3 kb) *R26RLacZ* mice at 14 dpf. X-gal staining revealed LacZ-positive cells in the cambium layer of the periosteum, but not in the BM (Supplemental Figure 5, D and F). Furthermore, we observed a large number of LacZ-positive cells in the external callus, in particular, in regions of hard

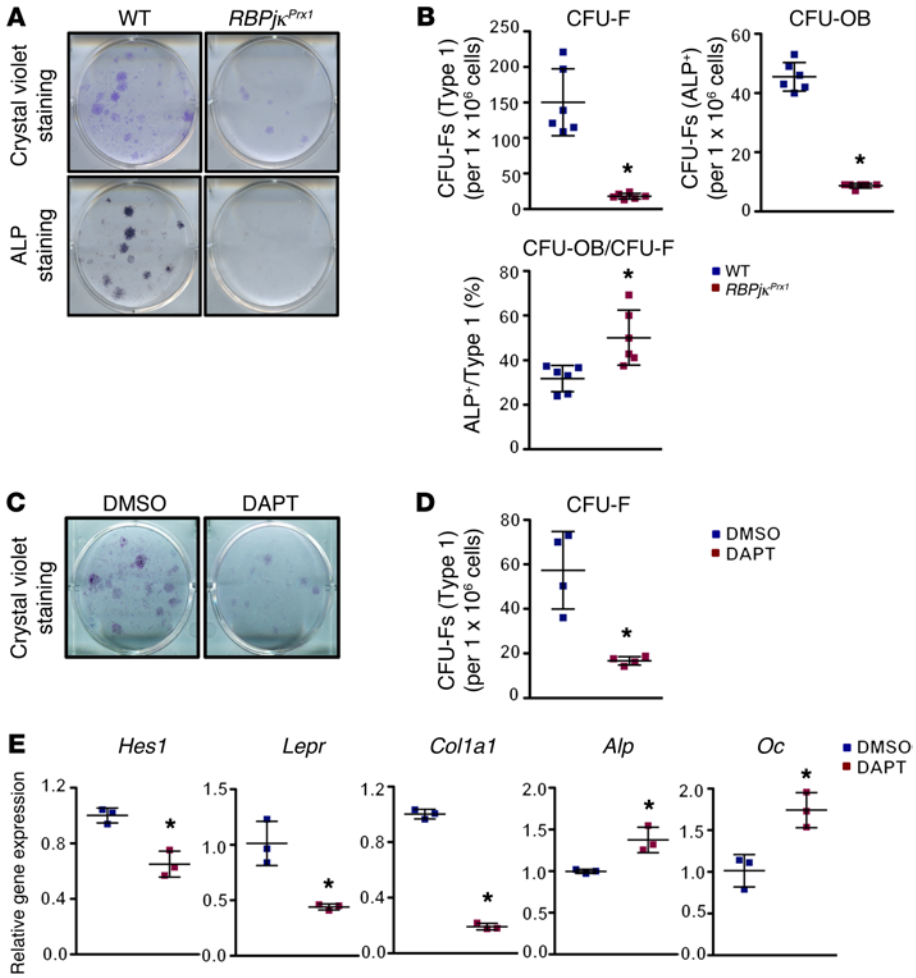

Figure 4. Fracture nonunions observed in *RBPjκ*^{Prx1} mutants are likely due to the significant reduction of BMSC numbers and altered differentiation status. (**A**) CFU-F assays on BMSCs isolated from WT and *RBPjκ*^{Prx1} mutant fractures at 42 dpf. Representative images for crystal violet staining of CFU-Fs and ALP staining of CFU-OBs are both shown. (**B**) *RBPjκ*^{Prx1} mutant fractures are associated with significantly reduced type 1 colonies (CFU-Fs) and ALP-positive colonies (CFU-OBs), but an increased ratio of CFU-OB to CFU-F. $n = 6$ mice per genotype. $^*P < 0.05$ compared with WT by 2-tailed, unpaired Student's *t* test. Results are expressed as mean ± SD. (**C**) CFU-F assays for BMSCs isolated from WT mice at 2 months of age and treated with either DMSO or DAPT for 14 days beginning on their third day in culture. Representative images for crystal violet staining of CFU-Fs are shown. (**D**) Quantification of DMSO- and DAPT-treated BMSC cultures show significantly reduced type 1 colonies (CFU-Fs). $^*P < 0.05$ compared with DMSO control by 2-tailed, unpaired Student's *t* test. Results are expressed as mean ± SD of 4 independent experiments. (**E**) Relative gene expression for *Hes1*, *Lepr*, *Col1a1*, *Alp*, and *Oc* in DAPT-treated BMSCs as compared with DMSO-treated control. $^*P < 0.05$, compared with DMSO control by 2-tailed, unpaired Student's *t* test. Results are expressed as mean ± SD of 3 independent experiments.

calluses. In contrast, no LacZ-positive cells were detected within the developing internal callus (Supplemental Figure 5, H and J). These results indicate that *Col1a1*(2.3 kb)–expressing osteoblasts in the periosteum only contribute to the formation of the external callus, but not the internal callus. We next analyzed fractures from mice with NOTCH signaling selectively removed from osteoblasts using the *Col1a1-Cre*(2.3 kb) transgenic line (*Col1a1-Cre*(2.3 kb)*; RBPjk*$^{fl/fl}$, hereafter *RBPjκ*^{Col1}). Western blot analyses confirmed that RBPjκ was efficiently deleted in osteoblasts of *RBPjκ*^{Col1} mice (Supplemental Figure 6). We then performed nonstabilized tibia fractures on *RBPjκ*^{Col1} or *RBPjk*$^{fl/fl}$ (WT control) mice. No significant differences in fracture repair between the 2 groups were revealed by any of the analyses, including radiographic, μCT, histological, and histomorphometric assessments (Figure 5). We also detected comparable CFU-Fs and CFU-OBs in the BM from *RBPjκ*^{Col1} mutant fractures and controls at 42 dpf, indicating that the BMSCs in *RBPjκ*^{Col1} mutants were unaffected by loss of NOTCH signaling in maturing osteoblasts (Supplemental Figure 7). These data demonstrate that *RBPjκ*^{Col1} mutant mice, in which NOTCH signaling is selectively removed in mature osteoblasts, are capable of normal fracture repair.

To determine whether loss of NOTCH signaling in fracture callus chondrocytes could also lead to fracture nonunion similar to that observed in *RBPjκ*^{Prx1} mutants, we performed nonstabilized tibia fractures on tamoxifen-inducible (TM-inducible) *Aggrecan-Cre*^{ERT2} *RBPjk*$^{fl/fl}$ (hereafter *RBPjκ*^{AcanTM}) and WT control mice at 2 months of age. *RBPjκ*^{AcanTM} and WT mice received TM (1 mg/10 g body weight) via intraperitoneal injections at 3, 5, 7, and 9 dpf to induce recombination of *RBPjk* floxed alleles following initiation of fracture repair during the chondrogenic or endochondral phase. Radiographs showed the initiation of mineralized callus at 14 dpf and complete bridging and bony union in both WT and *RBPjκ*^{AcanTM} mutant mice by 28 dpf (Figure 6A). IHC analyses from WT and *RBPjκ*^{AcanTM} fracture calluses at 10 dpf during the endochondral phase confirmed an extremely efficient removal of RBPjκ specifically from within chondrocytes and not adjacent mesenchymal/osteogenic tissue (Figure 6B). Histological analyses at both 10 and 28 dpf further confirmed the radiographic results and demonstrated that *RBPjκ*^{AcanTM} mutant mice undergo normal fracture repair processes with timely bony union (Figure 6B). Collectively, these data demonstrate that NOTCH signaling is dispensable in the differentiated cell lineages of osteoblasts or chondrocytes during fracture repair, while NOTCH signaling in the earliest skeletal progenitors is absolutely required for normal bone healing and unification.

Insufficient fracture stabilization is not required for fracture nonunion observed in RBPjκ^{Prx1} *mutants*. To exclude the possibility that fracture nonunion observed in *RBPjκ*^{Prx1} mutants was promoted by insufficient stabilization, we employed a rigidly stabilized femur osteotomy model. Two different gap sizes (1.2 mm and 0.66 mm)

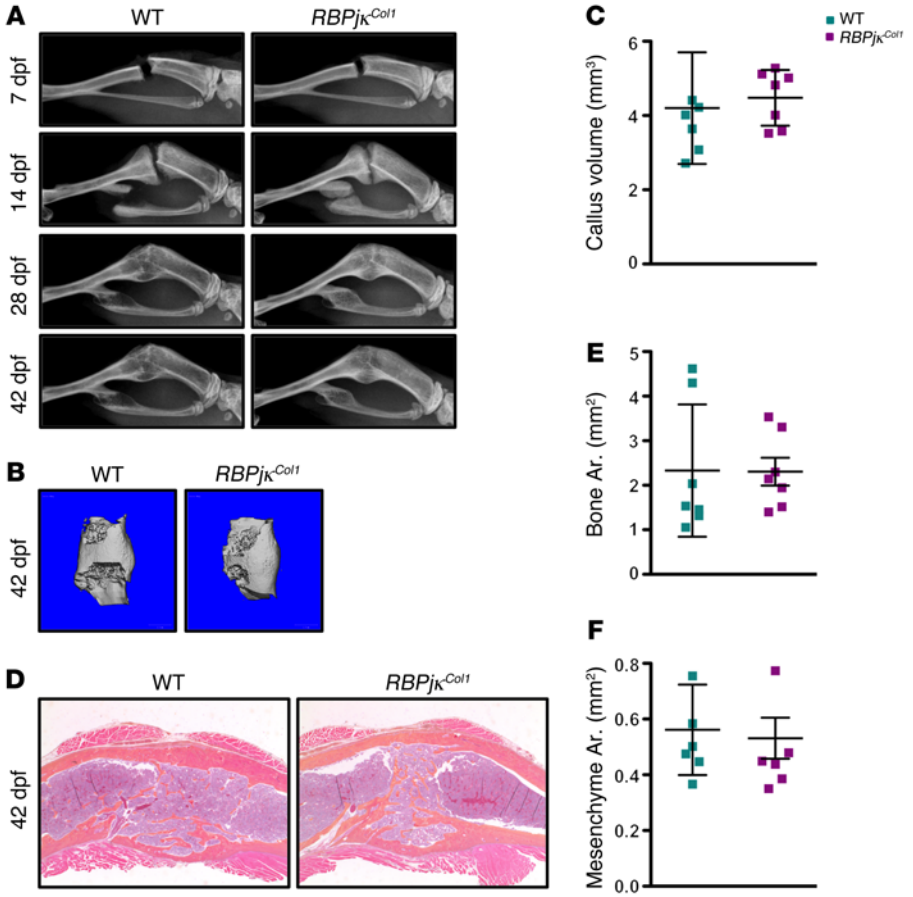

Figure 5. Loss of NOTCH signaling in mature osteoblasts does not lead to fracture nonunion. (**A**) A real-time radiographic comparison of 2 representative nonstabilized tibia fractures from WT and *RBPjκ*^{Col1} mutant mice at 0, 14, 28, and 42 dpf revealed normal fracture repair in *RBPjκ*^{Col1} mutants. n = 7 mice per genotype. (**B**) Representative μCT images of fracture calluses from WT and *RBPjκ*^{Col1} mutants at 42 dpf. n = 7 mice per genotype. $^*P < 0.05$ compared with WT by 2-tailed, unpaired Student's t test. Results are expressed as mean ± SD. (**C**) Reconstruction of μCT data revealed a similar amount of mineralized calluses between WT and *RBPjκ*^{Col1} mutants at 42 dpf. (**D**) ABH/OG-stained callus sections from *RBPjκ*^{Col1} mutants and controls at 42 dpf. Original magnification, ×2.5. (**E** and **F**) Histomorphometric analyses of ABH/OG-stained callus sections indicated no significant differences in bone and mesenchyme area between WT and *RBPjκ*^{Col1} mutant fractures. n = 7 mice per genotype. $^*P < 0.05$ compared with WT by 2-tailed, unpaired Student's t test. Results are expressed as mean ± SD.

of osteotomy were created in femurs of *RBPjκ*^{Prx1} mutants and WT controls and stabilized with a rigid internal fixator. By 14 dpf, radiographs revealed complete periosteal bridging in the control mice with a 1.2-mm osteotomy. In contrast, although the osteotomy gap narrowed and obscured on radiographs, radiolucent space could still be observed at 42 dpf in *RBPjκ*^{Prx1} mutant femurs (Figure 7A). Three-dimensional reconstructed μCT images also demonstrate impaired healing and nonunion in *RBPjκ*^{Prx1} mutant femurs (Figure 7B). Quantitatively, the bony callus within the 1.2-mm defect, representing the volume of the internal callus, was significantly lower in the *RBPjκ*^{Prx1} mutants. The values of the minimum polar moment of inertia (PMOI) (0.76 mm^4) were significantly less than those of controls (4.60 mm^4), indicating a lack of bone union and a high propensity of failure (Figure 7, C and D). Histologically, at 42 dpf, the 1.2-mm WT osteotomies exhibited complete continuity of the cortex with mature lamellar structure and normal BM, whereas no healing was evident in *RBPjκ*^{Prx1} mutants. In place of normal healing, *RBPjκ*^{Prx1} mutant osteotomies developed a cap-like structure sealing the medullary canal. Often, one segment would have some mineralization and bone formation near the osteotomy site, while the other was occupied by loose, fibrous tissue (Figure 7E). IHC for COL3A1 on 42 dpf mutant osteotomy sections further confirmed the fibrotic nature of the tissue within the osteotomy gap (Figure 7E).

For the 0.66-mm osteotomies, autoradiographs indicated bony bridging in the control group at 14 dpf; however, by 21 dpf, the *RBPjκ*^{Prx1} mutants still exhibited a radiolucent area at the level of the osteotomy (Supplemental Figure 8A). μCT scanning showed the same pattern of defective repair as observed in the autoradiographs (Supplemental Figure 8B). Histological analysis at 21 dpf demonstrated that new mineral deposition bridged the osteotomy gap, and islands of disorganized bone formed in the marrow space of WT controls. Alternatively, by 21 dpf, only one side of the bone fragments displayed bridging in *RBPjκ*^{Prx1} mutants, with small islands of mineralized trabecular bone in the intramedullary cavity. The opposing cortical bone did not show signs of healing or callus formation (Supplemental Figure 8C), indicating that the mutant osteotomy resulted in incomplete and inappropriate bridging. Therefore, osteotomies in *RBPjκ*^{Prx1} mutants developed either incomplete unions or nonunions, suggesting that insufficient stabilization is not required for fracture nonunion to occur, although defect size may contribute to the healing outcome.

Discussion

NOTCH signaling is a recently established pathway critical to skeletal development and disease in both mice (15, 16, 19–25) and humans (26–28). Fracture-repair mechanisms are believed to recapitulate a series of spatiotemporal cellular and signaling events that occur during skeletal development (29, 30), suggesting a potential involvement of NOTCH signaling. Evidence that further implicates NOTCH in the general processes of fracture repair has recently emerged, including: (a) an upregulation of some NOTCH components in murine callus tissues during fracture healing (31), (b) a downregulation of NOTCH signaling specifi-

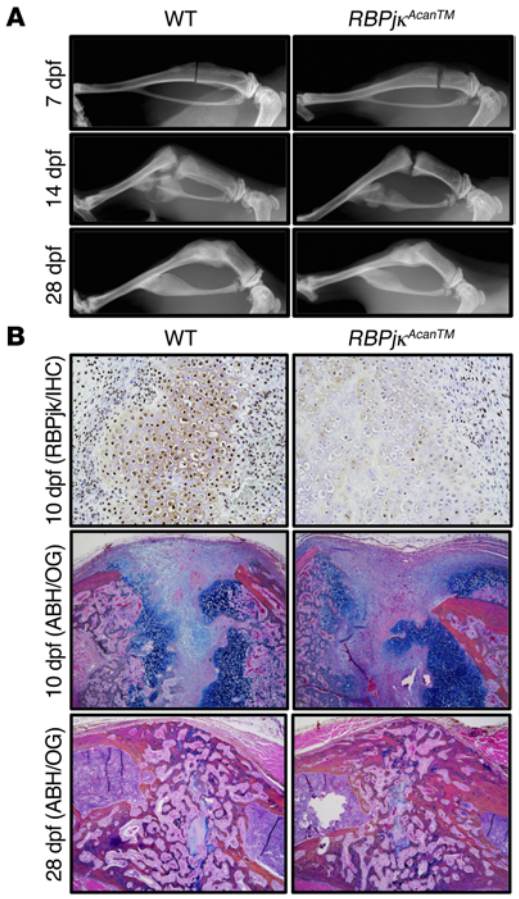

Figure 6. Loss of NOTCH signaling in fracture callus chondrocytes does not result in fracture nonunion. (**A**) A real-time radiographic comparison of 2 representative nonstabilized tibia fractures from WT and *RBPjκ*^{AcanTM} mutant mice at 0, 14, and 28 dpf, revealed normal fracture repair in *RBPjκ*^{AcanTM} mutants. *n* = 5 mice per genotype per time point. (**B**) IHC- and ABH/OG-stained callus sections from *RBPjκ*^{AcanTM} mutants and controls at 10 and 28 dpf. IHC analyses for RBPjκ shows an extremely efficient removal of RBPjk protein in *RBPjκ*^{AcanTM} mutant cartilage calluses. ABH/OG-stained callus sections indicate no identifiable tissue or cellular alterations in fracture repair between WT and *RBPjκ*^{AcanTM} mutant fractures. *n* = 5 mice per genotype per time point. Original magnification, ×20 (IHC); ×5 (ABH/OG).

cally within certain mouse skeletal progenitors during early fracture repair (32), and (c) evidence that systemic downregulation of NOTCH signaling just prior to fracture prolongs the inflammatory phase and alters fracture healing in mice (33). While these studies have implicated NOTCH in the fracture-repair process, the precise role of NOTCH within specific cell lineages remained unknown. Our findings here provide what we believe is the first genetic evidence that NOTCH signaling removal specifically within skeletal progenitors results in clonogenic BMSC depletion and fracture nonunion, while NOTCH removal in maturing osteoblasts and chondrocytes leads to no impairment in fracture healing and bone unification (34, 35). Our use of multiple fracture modalities and multiple gene targeting approaches has proven the requisite role for BMSCs and NOTCH signaling within BMSCs during fracture repair, irrespective of fracture stability and vascularization. Collectively, our work implicates both defective NOTCH signaling and BMSCs as possible causes of the failed or inappropriate intramedullary callus formation leading to fracture nonunions.

Current dogma suggests that various skeletal progenitors are recruited to the fracture site during bone repair, with at least 2 likely participants being BMSCs and PSCs (36, 37). Fracture callus development is known to occur at 3 specific loci: the medullary canal, the area between fractured cortices, and the extramedullary space, including the subperiosteal layer and surrounding soft tissues (13, 14). However, the precise identity of cells contributing to callus development and their relative contribution are not well defined. It is difficult to distinguish the precise role of various skeletal progenitors during fracture repair, partly due to the complex nature of the fracture-healing process, but also due to the lack of specific progenitor markers. Thus far, studies assessing the contribution of progenitor sources to bone healing have largely relied on transplantation approaches (13, 14, 38–41). In vivo lineage analyses using transplanted live bone grafts have demonstrated that the periosteum supports endochondral ossification, while BM/endosteum supports intramembranous ossification during bone repair (40). Periosteal progenitors give rise solely to skeletal cells specifically localized within the developing external callus (39, 40). Alternatively, reporter-tagged BM/BMSC transplantations have demonstrated that BMSCs localize to the fracture gap and may contribute to intramedullary or internal callus formation (13, 14). Based on these and other findings, we speculate that skeletal progenitors derived from the periosteum and BM/endosteum contribute differently to bone healing. While PSCs establish the external callus to provide rapid stability to the fracture via endochondral ossification, BMSCs might act to form the internal callus via intramembranous ossification and contribute markedly to fracture unification. Consistent with this hypothesis, the *RBPjκ*^{Prx1} mutant fractures show a relatively normal periosteal response with robust external callus formation, but fail to produce an internal callus and bone union, likely due to the depletion of local BMSC populations.

Since our study utilized a constitutively expressed *Prx1-Cre* transgene for the removal of NOTCH signaling in skeletal progenitors throughout skeletal development, it remains a question as to precisely when NOTCH signaling is required within skeletal progenitors during fracture repair. It may be that NOTCH signaling is required throughout development to maintain a functional pool of BMSCs or skeletal progenitors that are ultimately needed following skeletal injury for appropriate and complete fracture repair, or alternatively, NOTCH signaling may be required within BMSCs or skeletal progenitors strictly at the time of fracture repair in order to provide the appropriate cues directing bone unification. Parsing these differences will require the identification of precisely which skeletal progenitors or BMSC populations exhibit functionally relevant NOTCH signaling and will also require the development or use of appropriate inducible *Cre*-expressing transgenic mouse lines. As we develop these tools, future studies will also examine whether these particular NOTCH-deficient fracture nonunions can be repaired via the transplantation of appropriate BMSC populations at appropriate cell concentrations with appropriate cell carriers or scaffolds. Further development of these tools and data will aid in establishing the critical nature of NOTCH signaling within specific BMSC populations that are required for normal fracture

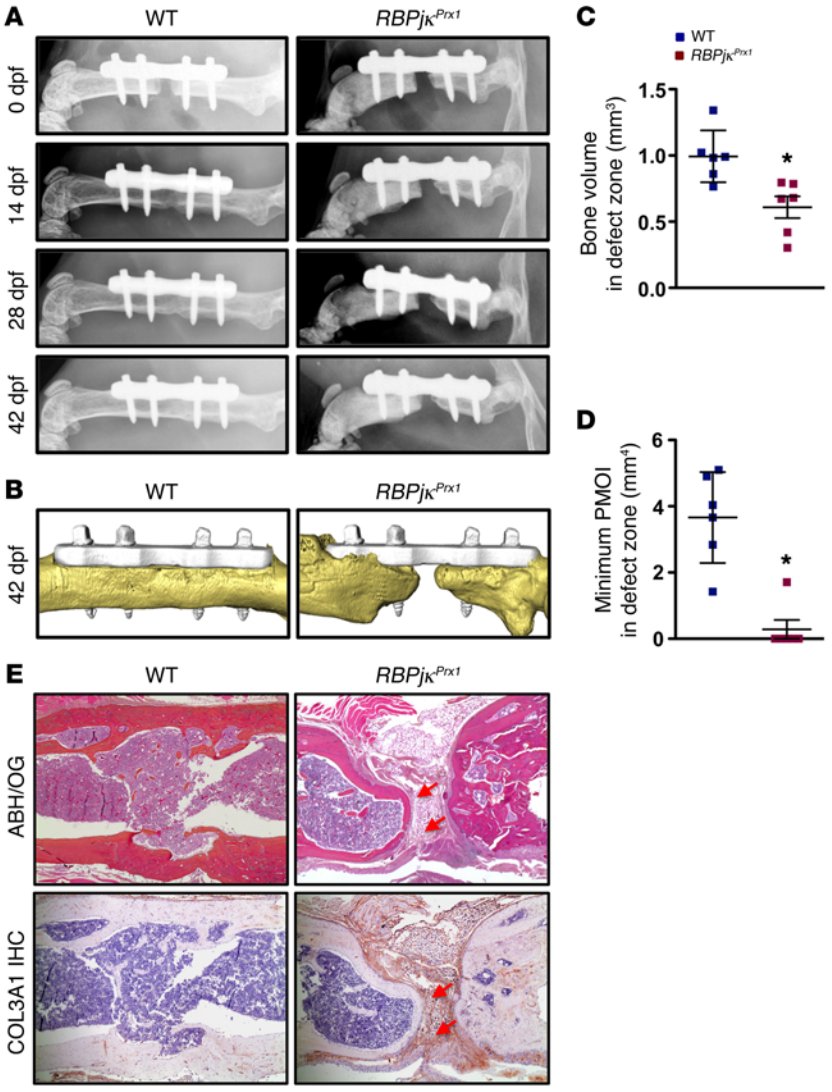

Figure 7. Insufficient fracture stabilization is not absolutely required for the fracture nonunion observed in *RBPjκ*^{Prx1} mutants. (**A**) A real-time radiographic comparison of 1.2-mm osteotomies in WT and *RBPjκ*^{Prx1} mutants. n = 6 mice per genotype. (**B**) Representative μCT images of 1.2-mm osteotomies in WT and *RBPjκ*^{Col1} mutants at 42 dpf. n = 6 mice per genotype. (**C** and **D**) Amira analyses of μCT data revealed significantly lower bone volume and minimum PMOI in defect zone. n = 6 mice per genotype. *$P < 0.05$ compared with WT by 2-tailed, unpaired Student's t test. Results are expressed as mean ± SD. (**E**) ABH/OG staining and IHC for COL3A1 staining on femur fracture sections (1.2-mm osteotomy) from WT and *RBPjκ*^{Prx1} mutants at 42 dpf revealed the formation of mesenchymal-like fibrous tissue (red arrows) in the 1.2-mm gap. n = 6 mice per genotype. Original magnification, ×5.

repair and unification and may also provide the basis for developing cell- and/or molecular-based therapeutics aimed at challenging skeletal repair and nonunion scenarios.

Fracture nonunions remain a challenging problem in orthopedic surgery. Traditionally, fracture nonunions have been classified as hypertrophic and atrophic. Hypertrophic nonunions are often associated with inadequate mechanical stabilization; therefore, immobilization alone may be sufficient for treatment. However, for atrophic nonunions and a distressing number of cases of hypertrophic nonunions that do not heal after appropriate surgical intervention, the causes have not been explicitly defined, and treatment options are limited. Many nonunion animal models are currently available; however, most of these models rely on creating critical-sized segmental defects (42, 43) or removing periosteum and BM (44, 45). These models infrequently simulate the clinical human scenario and rarely reflect the mechanisms for nonunions occurring in patients. In this study, we identified a genetic mouse model for both hypertrophic and atrophic nonunions. Specifically, we have demonstrated that nonstabilized fractures in *RBPjκ*^{prx1} mutants display (a) a persistent fracture line, (b) no bridging callus formation between cortices, (c) fibrosis within the fracture gap, and (d) poor biomechanical performance, all of which are consistent with the clinical assessment of human hypertrophic nonunions. Furthermore, we observed persistence of the osteotomy gap and osseous capping of the intramedullary canal in rigidly stabilized fractures of *RBPjκ*^{prx1} mice, which represent endpoint characteristics of atrophic nonunions (2, 46). Therefore, these results support the concept that BMSCs and potentially NOTCH signaling are key cellular and signaling participants in the pathogenesis of both hypertrophic and atrophic nonunion.

Fracture nonunions are sometimes considered to be avascular, although recent data suggest that no statistically significant change in the median vessel counts of biopsies from the fracture gap of patients with healing fractures, hypertrophic nonunions, or atrophic nonunions can be identified (47). These findings are supported by preclinical models, which have demonstrated the highly vascular nature of many nonunions, including atrophic nonunions (48, 49). Our study further demonstrates that internal callus formation can fail and fracture nonunion can occur, even in the presence of a well-vascularized fracture. Collectively, these data have extended our understanding of the pathophysiology of fracture nonunions and suggest that the fracture nonunions characterized here are likely due to the biological impairment of local skeletal progenitors at the fracture site or their depletion and that NOTCH signaling in particular is a key regulator.

It is of note that children with Alagille syndrome caused by *JAG1* or *NOTCH2* mutations have an especially high risk of lower extremity fractures, originally thought to be due to altered bone development and metabolism brought on by improper calcium, vitamin, and mineral regulation and/or altered osteoblast differentiation or function (50). Management of these pathological lower extremity fractures in Alagille syndrome patients can sometimes be challenging, with reports of recurrent fractures in some patients and poor healing outcomes and/or postfracture deformities in others (50, 51). Therefore, it may be important to assess BMSC status and CFU-F frequency in the BM of Alagille patients with complicated fracture repair scenarios and to consider BMSC or BM aspirate treatments to

enhance fracture repair. Furthermore, based on our findings, it may be relevant to establish the NOTCH signaling status within BMSCs and CFU-F frequency in all cases of prolonged fracture nonunion, especially when fractures do not heal even after appropriate surgical intervention, as it may be that these individuals have deficient or defective NOTCH signaling within their clonogenic populations of BMSCs.

Methods

Experimental animals. All mouse strains, including *RBPjk*$^{fl/fl}$, *Prx1-Cre*, and *Col1a1-Cre*(2.3 kb), have been described previously (52–54). *Prx1-Cre RBPjk*$^{fl/fl}$, *Prx1-Cre R26RLacZ*$^{fl/fl}$, *Col1a1-Cre*(2.3 kb) *RBPjk*$^{fl/fl}$, *Col1a1-Cre*(2.3 kb) *R26RLacZ*$^{fl/fl}$, and *Acan-Cre*^{ERT2} *RBPjk*$^{fl/fl}$ mice were viable and produced in Mendelian ratios. Mice were fractured at 8 to 10 weeks of age. *Acan-Cre*^{ERT2} *RBPjk*$^{fl/fl}$ mice received TM (1 mg/10 g body weight) via intraperitoneal injections on 3, 5, 7, and 9 dpf.

Fracture model. Prior to surgery, mice were anesthetized with 2.5% avertin (15 μl/g body weight) injected intraperitoneally. In the nonstabilized tibia fracture model, after the mice were anesthetized, an incision along the anterior side of the tibia was made. A transverse osteotomy was unilaterally performed at the mid-shaft of the tibia with a rotary bone saw. Fractured bones were repositioned without fixation, and the incision was closed. In the rigidly stabilized femur-fracture model, the right femur was exposed by a direct lateral approach, and a 4-hole titanium plate was installed across the anterolateral surface using 4 titanium screws (55) (RISystem). For the 0.66-mm defect, a transverse osteotomy was cut through the femoral middiaphysis using a 0.66-mm wire Gigli saw and a cutting guide (RISystem). The 1.2-mm osteotomy was created by making 2 transverse cuts with a 0.22-mm wire Gigli saw and a cutting guide. The wound was closed, and the bone was allowed to heal for up to 6 weeks. Following surgery, mice were kept in cages after recovery from anesthesia, allowing free unrestricted weight bearing, and buprenorphine was administered subcutaneously (0.1 mg/kg) to manage pain every 6 to 12 hours, beginning at the time of sedation, for up to 3 days following surgery. Fractures were confirmed immediately after surgery, and healing of the fractures was monitored weekly after fracture under anesthesia using a Faxitron Cabinet X-Ray System (Faxitron X-Ray Corp.).

μCT assessment of the mineralized callus and biomechanical torsion testing. After careful dissection, repaired tibiae and femurs from days 14, 28, and 42 were imaged using a μCT system (VivaCT 40, Scanco Medical), with an integration time of 300 ms, a current of 145 mA, and an energy setting of 55 kV. The threshold was chosen using 2D evaluation of several slices in the transverse anatomic plane so that mineralized callus was identified, but surrounding soft tissue was excluded. Quantification for the volumes of the bony calluses was determined as previously described using Scanco analysis software (56).

μCT image processing and analysis was also performed using Amira software (Amira 5.4.5, FEI Visualization Sciences Group). The volume of newly formed bone was measured from the 1.2-mm region (114 slices) that corresponded with the initial osteotomy after applying a bone mineral density threshold of 435 mg HA/cm^3 to binarize the image. Additionally, the PMOI, which is correlated with the bone's resistance to twisting, was calculated for each slice within the 1.2-mm defect region. The mean PMOI of the minimum 10% of slices was reported, as this is more indicative of the bone's lack of union or propensity to fail. Specimens with no bone growth for 11 consecutive slices possessed PMOI values of zero, but other specimens that were visually nonunified may have possessed nonzero PMOI values.

After μCT imaging of the fracture calluses, the specimens were moistened with PBS and frozen at –20°C until thawed for biomechanical testing as previously described (57). Briefly, specimens were potted in polymethyl methacrylate (PMMA) bone cement (DePuyOrthopaedics Inc.) in square aluminum tube holders and allowed to rehydrate in PBS at room temperature for 1 to 2 hours. Specimens were tested in torsion using an EnduraTec TestBench system (200 N.mm torque cell; Bose Corp.) at 1°/s until failure. The torque data were plotted against the rotational deformation to determine the maximum torque, torsional rigidity, and energy to maximum.

Analysis of mouse tissue sections. From 5 to 7 specimens (tibia or femur) in each group obtained at all time points were harvested, fixed in 10% neutral buffered formalin for 3 days, decalcified in 14% EDTA (pH 7.2) for 10 to 14 days, paraffin processed, embedded, and sectioned at a thickness of 3 μm. Sections were stained using ABH/OG staining and TRAP in order to analyze the cartilage composition and osteoclast formation in the fracture callus tissues. IHC stainings for COL3A1 (Abcam, ab7778) and RBPjκ (Cell Signaling) were performed on paraffin sections following the traditional antigen retrieval and colorimetric development methodologies. Tissues prepared for frozen sections were fixed in 4% PFA for 2 hours at 4°C, decalcified with 14% EDTA at 4°C for 10 days, infiltrated with gradient sucrose for 3 days, embedded with Tissue-Tek OCT medium, and sectioned at a thickness of 10 μm. LacZ staining and IF for PECAM (BD Biosciences, 550274) were performed on frozen sections. Cartilage area, bone area, mesenchyme area, and OC.S./B.S. were quantified on ABH/OG-stained and TRAP-stained sections using the Visiopharm Integrator System (Visiopharm).

CFU and molecular assays. BMSCs were isolated from fractured mice at 42 dpf or from WT mice at 2 months of age. Femurs and tibiae were removed and BM cells were flushed from the marrow cavity. Cells were plated at a density of 1×10^6 cells/well in 6-well tissue culture plates for 14 days without change of mouse MSC medium (Stem Cell Technologies). DAPT/DMSO-treated cultures were grown in standard mouse MSC medium for 3 days and then supplemented with DAPT (10 μM) or DMSO vehicle control for an additional 14 days. On either day 14 or 17 after plating, cells were fixed for crystal violet and/or ALP staining. Type I colonies (CFU-F), as previously described (15), and ALP-positive colonies (CFU-OB) were scored. RNA was isolated using the RNeasy Mini Kit (QIAGEN) according to the manufacturer's instructions. Real-time quantitative PCR (qPCR) was performed to analyze relative gene expression using the Bio-Rad CFX Connect Real-Time qPCR System. Gene expression was normalized to β-actin prior to being normalized to control samples. Mouse primers for *Hes1*, *Lepr*, *Col1a1*, *Alp*, *Oc*, and β-actin are listed in Supplemental Table 1.

Western blot. Bone proteins were extracted from femora and tibiae of *Prx1-Cre RBPjk*$^{fl/fl}$, *Col1a1-Cre; RBPjk*$^{fl/fl}$, and control mice with RIPA buffer supplemented with protease inhibitors and phosphatase inhibitors (Thermo Scientific, 78440) after BM cells were flushed away. Proteins were fractionated in an SDS-PAGE gel, transferred to a nitrocellulose membrane, and detected with the RBPjκ antibody (Cell Signaling, 5313).

Statistics. All results are presented as the mean ± SD. Comparisons between 2 groups were analyzed using 2-tailed, unpaired Student's *t* test. Two-way ANOVA followed by Dunnett's post hoc test was used for comparison of 2 groups at multiple time points. $P < 0.05$ was considered statistically significant.

Study approval. All animal studies were approved by the University of Rochester Committee on Animal Resources and the Duke University Institutional Animal Use and Care Committee.

Author contributions

CW conducted experiments, acquired data, analyzed data, and wrote the manuscript. JAI, AJM, YR, JS, and ZL conducted experiments, acquired data, and analyzed data. RJO and HAA assisted in experimental design, analyzed data, and edited the manuscript. MJH designed research studies, analyzed data, and wrote and edited the manuscript.

Acknowledgments

This work was supported in part by the following NIH grants: R01 grants (AR057022 and AR063071), an R21 grant (AR059733 to M.J. Hilton), a P50 Center of Research Translation grant (AR054041 to R.J. O'Keefe), and a P30 Core Center grant (AR061307 to M.J. Hilton and H.A. Awad). This work was also supported by a grant from the AOTrauma Research Clinical Priority Program on Bone Infection (to H.A. Awad). J.A. Inzana was supported by a National Science Foundation grant (NSF Award DGE-1419118). We would like to gratefully acknowledge the technical expertise and assistance of Sarah Mack, Kathy Maltby, Ashish Thomas, and Michael Thullen within the Histology, Biochemistry, and Molecular Imaging Core and the Biomechanics and Multimodal Tissue Imaging Core in the Center for Musculoskeletal Research at the University of Rochester Medical Center.

Address correspondence to: Matthew J. Hilton, Duke Orthopaedic Cellular, Developmental, and Genome Laboratories, Departments of Orthopaedic Surgery and Cell Biology, Duke University School of Medicine, 450 Research Drive, LSRC B321C, Durham, North Carolina 27710, USA. Phone: 919.613.9761; E-mail: matthew.hilton@dm.duke.edu.

1. Einhorn TA. Enhancement of fracture-healing. *J Bone Joint Surg Am*. 1995;77(6):940–956.
2. Marsh D. Concepts of fracture union, delayed union, and nonunion. *Clin Orthop Relat Res*. 1998;(355 Suppl):S22–S30.
3. Praemer A, Furner S, Rice DP. *Musculoskeletal Conditions in the United States*. Park Ridge, Illinois, USA: American Academy of Orthopaedic Surgeons; 1999.
4. Gaston MS, Simpson AH. Inhibition of fracture healing. *J Bone Joint Surg Br*. 2007;89(12):1553–1560.
5. Hernigou P, Beaujean F. [Bone marrow in patients with pseudarthrosis. A study of progenitor cells by in vitro cloning]. *Rev Chir Orthop Reparatrice Appar Mot*. 1997;83(1):33–40.
6. Seebach C, Henrich D, Tewksbury R, Wilhelm K, Marzi I. Number and proliferative capacity of human mesenchymal stem cells are modulated positively in multiple trauma patients and negatively in atrophic nonunions. *Calcif Tissue Int*. 2007;80(4):294–300.
7. Marcacci M, et al. Stem cells associated with macroporous bioceramics for long bone repair: 6- to 7-year outcome of a pilot clinical study. *Tissue Eng*. 2007;13(5):947–955.
8. Quarto R, et al. Repair of large bone defects with the use of autologous bone marrow stromal cells. *N Engl J Med*. 2001;344(5):385–386.
9. Hernigou P, Mathieu G, Poignard A, Manicom O, Beaujean F, Rouard H. Percutaneous autologous bone-marrow grafting for nonunions. Surgical technique. *J Bone Joint Surg Am*. 2006;88(suppl 1 pt 2):322–327.
10. Hernigou P, Poignard A, Beaujean F, Rouard H. Percutaneous autologous bone-marrow grafting for nonunions. Influence of the number and concentration of progenitor cells. *J Bone Joint Surg Am*. 2005;87(7):1430–1437.
11. Hernigou P, Poignard A, Manicom O, Mathieu G, Rouard H. The use of percutaneous autologous bone marrow transplantation in nonunion and avascular necrosis of bone. *J Bone Joint Surg Br*. 2005;87(7):896–902.
12. Tseng SS, Lee MA, Reddi AH. Nonunions and the potential of stem cells in fracture-healing. *J Bone Joint Surg Am*. 2008;90(suppl 1):92–98.
13. Granero-Molto F, et al. Regenerative effects of transplanted mesenchymal stem cells in fracture healing. *Stem Cells*. 2009;27(8):1887–1898.
14. Ueno M, et al. Distribution of bone marrow-derived cells in the fracture callus during plate fixation in a green fluorescent protein-chimeric mouse model. *Exp Anim*. 2011;60(5):455–462.
15. Hilton MJ, et al. Notch signaling maintains bone marrow mesenchymal progenitors by suppressing osteoblast differentiation. *Nat Med*. 2008;14(3):306–314.
16. Tu X, et al. Physiological notch signaling maintains bone homeostasis via RBPjk and Hey upstream of NFATc1. *PLoS Genet*. 2012;8(3):e1002577.
17. Kopan R, Ilagan MX. The canonical Notch signaling pathway: unfolding the activation mechanism. *Cell*. 2009;137(2):216–233.
18. Zhou BO, Yue R, Murphy MM, Peyer JG, Morrison SJ. Leptin-receptor-expressing mesenchymal stromal cells represent the main source of bone formed by adult bone marrow. *Cell Stem Cell*. 2014;15(2):154–168.
19. Dong Y, et al. RBPjκ-dependent Notch signaling regulates mesenchymal progenitor cell proliferation and differentiation during skeletal development. *Development*. 2010;137(9):1461–1471.
20. Kohn A, et al. Cartilage-specific RBPjκ-dependent and -independent Notch signals regulate cartilage and bone development. *Development*. 2012;139(6):1198–1212.
21. Engin F, et al. Dimorphic effects of Notch signaling in bone homeostasis. *Nat Med*. 2008;14(3):299–305.
22. Mead TJ, Yutzey KE. Notch pathway regulation of chondrocyte differentiation and proliferation during appendicular and axial skeleton development. *Proc Natl Acad Sci U S A*. 2009;106(34):14420–14425.
23. Tao J, et al. Osteosclerosis owing to Notch gain of function is solely Rbpj-dependent. *J Bone Miner Res*. 2010;25(10):2175–2183.
24. Watanabe N, et al. Suppression of differentiation and proliferation of early chondrogenic cells by Notch. *J Bone Miner Metab*. 2003;21(6):344–352.
25. Zanotti S, Smerdel-Ramoya A, Stadmeyer L, Durant D, Radtke F, Canalis E. Notch inhibits osteoblast differentiation and causes osteopenia. *Endocrinology*. 2008;149(8):3890–3899.
26. Chapman G, Sparrow DB, Kremmer E, Dunwoodie SL. Notch inhibition by the ligand DELTA-LIKE 3 defines the mechanism of abnormal vertebral segmentation in spondylocostal dysostosis. *Hum Mol Genet*. 2011;20(5):905–916.
27. Guegan K, Stals K, Day M, Turnpenny P, Ellard S. JAG1 mutations are found in approximately one third of patients presenting with only one or two clinical features of Alagille syndrome. *Clin Genet*. 2012;82(1):33–40.
28. Majewski J, et al. Mutations in NOTCH2 in families with Hajdu-Cheney syndrome. *Hum Mutat*. 2011;32(10):1114–1117.
29. Vortkamp A, Pathi S, Peretti GM, Caruso EM, Zaleske DJ, Tabin CJ. Recapitulation of signals regulating embryonic bone formation during postnatal growth and in fracture repair. *Mech Dev*. 1998;71(1-2):65–76.
30. Ferguson C, Alpern E, Miclau T, Helms JA. Does adult fracture repair recapitulate embryonic skeletal formation? *Mech Dev*. 1999;87(1-2):57–66.
31. Dishowitz MI, Terkhorn SP, Bostic SA, Hankenson KD. Notch signaling components are upregulated during both endochondral and intramembranous bone regeneration. *J Orthop Res*. 2012;30(2):296–303.
32. Matthews BG, et al. Analysis of alphaSMA-labeled progenitor cell commitment identifies notch signaling as an important pathway in fracture healing. *J Bone Miner Res*. 2014;29(5):1283–1294.
33. Dishowitz MI, et al. Systemic inhibition of

canonical Notch signaling results in sustained callus inflammation and alters multiple phases of fracture healing. *PLoS One*. 2013;8(7):e68726.
34. Dacic S, Kalajzic I, Visnjic D, Lichtler AC, Rowe DW. Col1a1-driven transgenic markers of osteoblast lineage progression. *J Bone Miner Res*. 2001;16(7):1228–1236.
35. Kalajzic Z, et al. Directing the expression of a green fluorescent protein transgene in differentiated osteoblasts: comparison between rat type I collagen and rat osteocalcin promoters. *Bone*. 2002;31(6):654–660.
36. Utvag SE, Grundnes O, Reikeraos O. Effects of periosteal stripping on healing of segmental fractures in rats. *J Orthop Trauma*. 1996;10(4):279–284.
37. Ozaki A, Tsunoda M, Kinoshita S, Saura R. Role of fracture hematoma and periosteum during fracture healing in rats: interaction of fracture hematoma and the periosteum in the initial step of the healing process. *J Orthop Sci*. 2000;5(1):64–70.
38. Taguchi K, Ogawa R, Migita M, Hanawa H, Ito H, Orimo H. The role of bone marrow-derived cells in bone fracture repair in a green fluorescent protein chimeric mouse model. *Biochem Biophys Res Commun*. 2005;331(1):31–36.
39. Zhang X, et al. Periosteal progenitor cell fate in segmental cortical bone graft transplantations: implications for functional tissue engineering. *J Bone Miner Res*. 2005;20(12):2124–2137.
40. Colnot C. Skeletal cell fate decisions within periosteum and bone marrow during bone regeneration. *J Bone Miner Res*. 2009;24(2):274–282.
41. Colnot C, Huang S, Helms J. Analyzing the cellular contribution of bone marrow to fracture healing using bone marrow transplantation in mice. *Biochem Biophys Res Commun*. 2006;350(3):557–561.
42. Chaubey A, et al. Structural and biomechanical responses of osseous healing: a novel murine nonunion model. *J Orthop Traumatol*. 2013;14(4):247–257.
43. Liu K, et al. A murine femoral segmental defect model for bone tissue engineering using a novel rigid internal fixation system. *J Surg Res*. 2013;183(2):493–502.
44. Kokubu T, Hak DJ, Hazelwood SJ, Reddi AH. Development of an atrophic nonunion model and comparison to a closed healing fracture in rat femur. *J Orthop Res*. 2003;21(3):503–510.
45. Kaspar K, et al. A new animal model for bone atrophic nonunion: fixation by external fixator. *J Orthop Res*. 2008;26(12):1649–1655.
46. Harrison LJ, Cunningham JL, Stromberg L, Goodship AE. Controlled induction of a pseudarthrosis: a study using a rodent model. *J Orthop Trauma*. 2003;17(1):11–21.
47. Reed AA, Joyner CJ, Brownlow HC, Simpson AH. Human atrophic fracture non-unions are not avascular. *J Orthop Res*. 2002;20(3):593–599.
48. Brownlow HC, Reed A, Simpson AH. The vascularity of atrophic non-unions. *Injury*. 2002;33(2):145–150.
49. Reed AA, Joyner CJ, Isefuku S, Brownlow HC, Simpson AH. Vascularity in a new model of atrophic nonunion. *J Bone Joint Surg Br*. 2003;85(4):604–610.
50. Bales CB, et al. Pathologic lower extremity fractures in children with Alagille syndrome. *J Pediatr Gastroenterol Nutr*. 2010;51(1):66–70.
51. Nozaka K, Shimada Y, Miyakoshi N, Yamada S, Kasukawa Y, Noguchi A. Pathological fracture of the femur in Alagille syndrome that was treated with low-intensity pulsed ultrasound stimulation and an Ilizarov ring fixator: a case report. *BMC Musculoskelet Disord*. 2014;15:225.
52. Han H, et al. Inducible gene knockout of transcription factor recombination signal binding protein-J reveals its essential role in T versus B lineage decision. *Int Immunol*. 2002;14(6):637–645.
53. Logan M, Martin JF, Nagy A, Lobe C, Olson EN, Tabin CJ. Expression of Cre Recombinase in the developing mouse limb bud driven by a Prxl enhancer. *Genesis*. 2002;33(2):77–80.
54. Miao D, et al. Osteoblast-derived PTHrP is a potent endogenous bone anabolic agent that modifies the therapeutic efficacy of administered PTH 1-34. *J Clin Invest*. 2005;115(9):2402–2411.
55. Matthys R, Perren SM. Internal fixator for use in the mouse. *Injury*. 2009;40(suppl 4):S103–S109.
56. Reynolds DG, et al. muCT-based measurement of cortical bone graft-to-host union. *J Bone Miner Res*. 2009;24(5):899–907.
57. Xie C, et al. Structural bone allograft combined with genetically engineered mesenchymal stem cells as a novel platform for bone tissue engineering. *Tissue Eng*. 2007;13(3):435–445.